Optimal Damping with Hierarchical Adaptive Quadrature for Efficient Fourier Pricing of Multi-Asset Options in Lévy Models

Christian Bayer[1], Chiheb Ben Hammouda[*2], Antonis Papapantoleon[3], Michael Samet[†4] and Raúl Tempone[4,2]

[1]Weierstrass Institute for Applied Analysis and Stochastics (WIAS), Berlin, Germany.
[2]Chair of Mathematics for Uncertainty Quantification, RWTH Aachen University, Aachen, Germany.
[3]Delft Institute of Applied Mathematics, EEMCS, TU Delft, 2628 Delft, The Netherlands, and Department of Mathematics, SAMPS, NTUA, 15780 Athens, Greece and Institute of Applied and Computational Mathematics, FORTH, 70013 Heraklion, Greece.
[4]King Abdullah University of Science and Technology (KAUST), Computer, Electrical and Mathematical Sciences & Engineering Division (CEMSE), Thuwal, Saudi Arabia.

Abstract

Efficient pricing of multi-asset options is a challenging problem in quantitative finance. When the characteristic function is available, Fourier-based methods become competitive compared to alternative techniques because the integrand in the frequency space has often higher regularity than in the physical space. However, when designing a numerical quadrature method for most of these Fourier pricing approaches, two key aspects affecting the numerical complexity should be carefully considered: (i) the choice of the damping parameters that ensure integrability and control the regularity class of the integrand and (ii) the effective treatment of the high dimensionality. To address these challenges, we propose an efficient numerical method for pricing European multi-asset options based on two complementary ideas. First, we smooth the Fourier integrand via an optimized choice of damping parameters based on a proposed heuristic optimization rule. Second, we use sparsification and dimension-adaptivity techniques to accelerate the convergence of the quadrature in high dimensions. Our extensive numerical study on basket and rainbow options under the multivariate geometric Brownian motion and some Lévy models demonstrates the advantages of adaptivity and our damping rule on the numerical complexity of the quadrature methods. Moreover, our approach achieves substantial computational gains compared to the Monte Carlo method.

Keywords option pricing, Fourier methods, damping parameters, adaptive sparse grid quadrature, basket and rainbow options, multivariate Lévy models.

2010 Mathematics Subject Classification 65D32, 65T50, 65Y20, 91B25, 91G20, 91G60

*benhammouda@uq.rwth-aachen.de
†michael.samet@kaust.edu.sa

1 Introduction

Pricing multi-asset options, such as basket and rainbow options, is an interesting and challenging problem in quantitative finance because prices cannot be analytically computed in most cases; thus, efficient numerical methods are required. Moreover, despite the popularity of the Black–Scholes model, where the stock dynamics follow the geometric Brownian motion (GBM), Lévy models, such as the variance Gamma (VG) [45] and normal inverse Gaussian (NIG) models [3], have shown a remarkable fit to empirical market behavior [17, 52] by accounting for market jumps in prices, heavy tails, and high leptokurtosis.

Under the no-arbitrage assumption, option prices are given as expectations under an (equivalent) martingale measure and approximated using numerical integration methods. In this context, the prevalent numerical method is the Monte Carlo (MC) method [31], which has a convergence rate insensitive to the input space dimensionality and payoff regularity, except for multilevel MC methods [7], where Lipschitz continuity is necessary to obtain optimal convergence rates. However, the convergence may be very slow, and one may not exploit the available regularity structure to achieve better convergence rates. Another class of methods relies on deterministic quadrature methods whose performance highly depends on the input space dimension and integrand regularity. Some studies [6, 8] have combined adaptivity, sparsification techniques and hierarchical representations (Brownian bridge and Richardson extrapolation) with quadrature methods to treat the high dimensionality effectively. Moreover, financial payoffs usually have low regularity; therefore, analytic and numerical smoothing techniques were introduced for better convergence [9, 6, 10, 8]. All aforementioned improvements were performed in the physical space.

In this work, we propose a novel approach for pricing European multidimensional basket and rainbow[1] options under multivariate GBM and Lévy models. Compared to the previously mentioned approaches, we recover the higher regularity of the integrand by mapping the problem from the physical space to the frequency space, when the Fourier transforms of the payoff and density are well-defined and known explicitly. Moreover, when designing our method, we effectively treat two key aspects affecting the numerical complexity: (i) the choice of the damping parameters that ensure integrability and control the regularity class of the integrand and (ii) the high dimensionality of the integration problem. Based on the extension of the one-dimensional (1D) Fourier valuation formula [49, 41] to the multivariate case, first, we smooth the Fourier integrand via an optimal choice of the damping parameters based on a proposed heuristic optimization rule. Second, we use adaptive sparse grid quadrature (ASGQ) based on sparsification and dimension-adaptivity techniques, to accelerate the numerical quadrature convergence in high dimensions.

Fourier-based pricing methods [13, 49, 41, 23, 27, 42, 40, 38, 5] map the original problem to the frequency space and obtain the solution in the physical space using the Fourier inversion theorem. The approximation of the resulting integral is performed numerically using direct integration (DI) methods or the fast Fourier transform (FFT). The common ingredient for these approaches is the explicit knowledge of the characteristic function (i.e., the Fourier transform of the probability density function) corresponding to the price dynamics. There are three different popular Fourier valuation approaches. In the first approach, originally proposed by Carr and Madan, see [13, 39, 14], a Fourier transform is applied in the log-strike variable, k. Hence, for fixed maturity t, the whole

[1]Rainbow options [46] are appealing to investors because they allow the reduction of risk exposure to the market at a cheap cost by betting more on individual performance among a group of individual stocks than the overall performance of the portfolio stocks when considering basket options, for instance see [32].

curve of option prices, $C(t, \cdot)$, is computed. To ensure the existence of the Fourier transform, one must multiply the pricing function by an exponential damping factor with respect to (w.r.t.) the strike parameter. This method is appropriate for 1D problems; and extending it to the multi-asset option pricing context is difficult. The strike price is not defined for all stocks, whereas the multivariate density depends on all the underlyings. Moreover, the derivations must be performed separately for each payoff and stock dynamics. Given the characteristic function and Fourier transform of the payoff function, an alternative approach, see [49, 41, 34, 24], uses a highly modular pricing framework. This method separates the underlying stochastic process from the derivative payoff using the Plancherel–Parseval Theorem and uses the generalized inverse Fourier transform to obtain the option price. In addition, this approach introduces damping parameters w.r.t. the stock prices variables to ensure integrability, which shifts the integration contour to a parallel line to the real axis in the complex space. This technique is easier to extend to the multivariate case compared to the first approach in [13, 39, 14]. The third approach [27, 50, 60] relies on the Fourier cosine or sine series expansion of the density function in relation to the characteristic function. It is challenging to generalize this class of methods to the multidimensional setting because an analytic formula for the cosine or sine series coefficients of the payoff function cannot easily be obtained and should be recovered numerically. This numerical treatment influences the convergence rate of the method. Moreover, even though this approach does not introduce damping parameters to ensure integrability, truncation parameters must be determined. The method fails to converge when these truncation parameters are not chosen appropriately [35]. A practical choice in a high-dimensional setting remains a challenging open problem.

To the best of our knowledge, when using the second type Fourier valuation approach (as in [49, 41, 34, 24]), there is no precise analysis of the effect of the damping parameters on the convergence speed of quadrature methods or guidance on choosing them to improve the numerical performance, particularly in the multivariate setting. Previous works have set arbitrary choices for the damping parameter, and only [43, 36] studied the damping parameter selection for the first type Fourier valuation approach (as in [13, 39, 14]) in the 1D setting to obtain robust integration behavior. In this work, when pricing basket and rainbow options under the multivariate GBM and Lévy models based on the extension of the one-dimensional Fourier valuation formula [49, 41] to the multivariate case, we demonstrate that the choice of the damping parameters highly affects the speed of convergence of the numerical quadrature. In addition, motivated by error estimates based on contour integration tools, we propose a general heuristic framework for the optimal choice of the damping parameters, which can be tailored and extended to various pricing models, resulting in a smoother integrand and improving the efficiency of the numerical quadrature. Based on this proposed heuristic rule, the vector of the optimal damping parameters can be obtained by solving a simple optimization problem. Moreover, we demonstrate the consistent advantage of the optimal damping rule through numerical examples with different dimensions and parameter constellations.

The numerical evaluation of the resulting inverse Fourier integral can be performed using the FFT algorithm [13, 18], which could be faster than DI methods because it exploits periodicities and symmetries. However, it cannot satisfy the requirement for matching the pricing algorithm to the structure of the market data and must be assisted by interpolation and extrapolation methods for the smile surface, in contrast to DI methods, which allow for flexible strikes (refer to Chapter 4 of [61] and [43] for further comparisons of FFT and DI). An additional downside of the FFT method is that it has an additional truncation error and requires the determination of the upper and lower truncation parameters of the integral. This task is nontrivial for multidimensional integrals because the speed of decay to zero of the integrand depends on the damping factors, which are unknown a priori, creating dependence between the truncation and damping parameters. In this work, we opt for the DI approach combined with an unbounded quadrature (Gaussian quadrature rule) to evaluate the option price. Investigating the optimal choice of the damping and truncation parameters for FFT when pricing multi-asset options remains for future work.

Through an extensive numerical study on basket and rainbow options under the multivariate GBM, VG, and NIG models, we demonstrate the advantages of adaptivity and our rule for choosing the damping parameters on the numerical complexity of the quadrature methods for approximating the Fourier valuation integrals. Moreover, we show that our approach achieves substantial computational gains over the MC method for different dimensions and parameter constellations.

Section 2 introduces the proposed pricing framework in the Fourier space and the multivariate valuation formula. In Section 3, we explain our methodology. In Section 3.1, we motivate and state our heuristic rule for choosing of the damping parameters. Moreover, we present the different hierarchical deterministic quadrature methods used for numerically evaluating the inverse Fourier integrals of interest in Section 3.2. Finally, in Section 4, we report and analyze the obtained results, illustrating the advantages of the proposed approach and highlighting the considerable computational gains achieved over the MC method.

2 Problem Setting and Pricing Framework

In this work, we are interested in efficiently computing the price of European d-asset options using Fourier valuation formulas. For concreteness, we concentrate on two specific examples, namely (i) basket put[2] and (ii) rainbow options, precisely the call on min. The respective payoffs of basket put and call on min are given, for $K > 0$, by:

$$(2.1)\quad (i)\ P(\mathbf{X}_T) = \max\left(K - \sum_{i=1}^{d} e^{X_T^i}, 0\right); \quad (ii)\ P(\mathbf{X}_T) = \max\left(\min\left(e^{X_T^1}, \ldots, e^{X_T^d}\right) - K, 0\right),$$

where $X_T^i := \log(S_T^i), i = 1, \ldots, d$, $\{S_T^i\}_{i=1}^d$ are the prices of the underlying assets at the maturity T, and $\mathbf{X}_T := \left(X_T^1, \ldots, X_T^d\right)$.

Moreover, $\overline{\widehat{P}}(\mathbf{u}) = \overline{\mathcal{F}[P(\mathbf{x})](\mathbf{u})} = \int_{\mathbb{R}^d} e^{-\mathrm{i}\langle \mathbf{u}, \mathbf{x}\rangle} P(\mathbf{x}) d\mathbf{x}$ denotes the conjugate of the Fourier transform, $\mathcal{F}[.]$ of $P(\cdot)$. We refer to [55, 41, 51] for the definition of the generalized Fourier transform and its properties. The conjugate of the payoff transform is given by (2.2) for the basket put and (2.3) for the call on min (for more details on the derivation we refer to Page 79 in [47] and Page 16 in [24]):

$$(2.2)\quad \overline{\widehat{P}}(\mathbf{z}) = K^{1-\mathrm{i}\sum_{j=1}^d z_j} \frac{\prod_{j=1}^d \Gamma\left(-\mathrm{i} z_j\right)}{\Gamma\left(-\mathrm{i}\sum_{j=1}^d z_j + 2\right)}, \quad \mathbf{z} \in \mathbb{C}^d,\ \Im[z_j] > 0\ \forall j \in \{1, \ldots, d\};$$

$$(2.3)\quad \overline{\widehat{P}}(\mathbf{z}) = \frac{K^{1-\mathrm{i}\sum_{j=1}^d z_j}}{\left(\mathrm{i}\left(\sum_{j=1}^d z_j\right) - 1\right)\prod_{j=1}^d \left(\mathrm{i} z_j\right)}, \quad \mathbf{z} \in \mathbb{C}^d,\ \Im[z_j] < 0\ \forall j \in \{1, \ldots, d\},\ \sum_{j=1}^d \Im[z_j] < -1,$$

[2] To simplify the presentation, we consider the unweighted basket put payoff. The generalization to the weighted case as presented in Section 4 can be done straightforwardly.

where $\Gamma(\cdot)$ denotes the complex Gamma function defined for complex numbers with a positive real part, $\Im(\cdot)$ denotes the imaginary part of a complex number, and i denotes the unit imaginary number.

For asset dynamics, we consider three models: (i) the multivariate GBM, and two Lévy models: (ii) the multivariate VG and (iii) multivariate NIG model. Appendix A presents a brief description of these models. Moreover, $\Phi_{\mathbf{X}_T}(\cdot)$ denotes the joint characteristic function of $\mathbf{X}_T$, with $\Phi_{\mathbf{X}_T}(\cdot) = e^{\mathrm{i}\langle \cdot, \mathbf{X}_0\rangle}\phi_{\mathbf{X}_T}(\cdot)$, where $\phi_{\mathbf{X}_T}(\cdot)$ is expressed in Table 2.1 for each pricing model, and $\langle ., .\rangle$ denotes the inner product on $\mathbb{R}^d$.

Model	$\phi_{\mathbf{X}_T}(\mathbf{z})$
GBM	$\exp\left(\mathrm{i}\langle \mathbf{z}, r\mathbf{1}_{\mathbb{R}^d} - \frac{1}{2}\operatorname{diag}(\mathbf{\Sigma})\rangle T - \frac{T}{2}\langle \mathbf{z}, \mathbf{\Sigma}\mathbf{z}\rangle\right), \quad \mathbf{z} \in \mathbb{C}^d,\ \Im[z] \in \delta_X$
VG	$\exp(\mathrm{i}\langle \mathbf{z}, r\mathbf{1}_{\mathbb{R}^d} + \boldsymbol{\mu}_{VG}\rangle T)\left(1 - \mathrm{i}\nu\langle \boldsymbol{\theta}, \mathbf{z}\rangle + \frac{1}{2}\nu\langle \mathbf{z}, \mathbf{\Sigma}\mathbf{z}\rangle\right)^{-T/\nu}, \quad \mathbf{z} \in \mathbb{C}^d,\ \Im[z] \in \delta_X$
NIG	$\exp\left(\mathrm{i}\langle \mathbf{z}, r\mathbf{1}_{\mathbb{R}^d} + \boldsymbol{\mu}_{NIG}\rangle T + \delta T\left(\sqrt{\alpha^2 - \langle \boldsymbol{\beta}, \mathbf{\Delta}\boldsymbol{\beta}\rangle} - \sqrt{\alpha^2 - \langle \boldsymbol{\beta} + \mathrm{i}\mathbf{z}, \mathbf{\Delta}(\boldsymbol{\beta} + \mathrm{i}\mathbf{z})\rangle}\right)\right),$ $\mathbf{z} \in \mathbb{C}^d,\ \Im[z] \in \delta_X$

Table 2.1: The expression of $\phi_{X_T}(\cdot)$ for the different pricing models. r is the interest rate, $\mathbf{1}_{\mathbb{R}^d}$ is the d-dimensional unit vector. δ_X is the strip of the regularity of the characteristic function and is given in Table 2.3 for each pricing model. Appendix A provides the definitions of the various model parameters.

We extend the 1D representation [41] to derive the pricing valuation formula in the Fourier space for the multivariate setting. By the virtue of the inverse generalized Fourier transform theorem, we express the payoff function, $P(\cdot)$, w.r.t. the conjugate of the payoff transform, $\overline{\widehat{P}}(\cdot)$:

$$P(\mathbf{x}) = \Re\left[\frac{1}{(2\pi)^d}\int_{\mathbb{R}^d + \mathrm{i}\mathbf{R}} e^{\mathrm{i}\langle \mathbf{u}, \mathbf{x}\rangle}\overline{\widehat{P}}(\mathbf{u})d\mathbf{u}\right],\ \mathbf{R} \in \overline{\delta}_P,\ \mathbf{x} \in \mathbb{R}^d, \tag{2.4}$$

where $\mathbf{R} \in \overline{\delta}_P \subset \mathbb{R}^d$ is the vector of damping parameters ensuring the integrability, $\overline{\delta}_P$ is the conjugate strip of analyticity of the payoff transform, presented for each payoff in Table 2.2. $\Re[\cdot]$ denotes the real part of a complex number.

Using (2.4) and Fubini's theorem, we obtain the multivariate Fourier valuation formula for the option price:

$$\begin{aligned}
V(\mathbf{\Theta}_m, \mathbf{\Theta}_p) &= e^{-rT}\mathbb{E}\left[P(\mathbf{X}_T)\right] = e^{-rT}\int_{\mathbb{R}^d} P(\mathbf{x})\rho_{\mathbf{X}_T}(\mathbf{x})d\mathbf{x}, \\
&= (2\pi)^{-d}e^{-rT}\mathbb{E}\left[\Re\left(\int_{\mathbb{R}^d + \mathrm{i}\mathbf{R}} e^{\mathrm{i}\langle \mathbf{u}, \mathbf{X}_T\rangle}\overline{\widehat{P}}(\mathbf{u})d\mathbf{u}\right)\right],\ \mathbf{R} \in \overline{\delta}_P \\
&= (2\pi)^{-d}e^{-rT}\Re\left(\int_{\mathbb{R}^d + \mathrm{i}\mathbf{R}} \mathbb{E}[e^{\mathrm{i}\langle \mathbf{u}, \mathbf{X_T}\rangle}]\overline{\widehat{P}}(\mathbf{u})d\mathbf{u}\right),\ \mathbf{R} \in \delta_V := \overline{\delta}_P \cap \delta_X \\
&= (2\pi)^{-d}e^{-rT}\Re\left(\int_{\mathbb{R}^d + \mathrm{i}\mathbf{R}} \Phi_{\mathbf{X_T}}(\mathbf{u})\overline{\widehat{P}}(\mathbf{u})d\mathbf{u}\right), \\
&= (2\pi)^{-d}e^{-rT}e^{-\langle \mathbf{R}, \mathbf{X}_0\rangle}\Re\left(\int_{\mathbb{R}^d} e^{\mathrm{i}\langle \mathbf{u}, \mathbf{X}_0\rangle}\phi_{\mathbf{X_T}}(\mathbf{u} + \mathrm{i}\mathbf{R})\overline{\widehat{P}}(\mathbf{u} + \mathrm{i}\mathbf{R})d\mathbf{u}\right), \\
&:= \int_{\mathbb{R}^d} g(\mathbf{u}; \mathbf{R}, \mathbf{\Theta}_m, \mathbf{\Theta}_p)d\mathbf{u}, \qquad (2.5)
\end{aligned}$$

where $\rho_{\mathbf{X}_T}(\cdot)$ is the risk-neutral conditional transition probability density function of $\mathbf{X}_T$, and $\mathbf{\Theta}_p$ denotes the vector of payofsf parameters. To ensure the L^1 integrability of $g(\cdot)$ in (2.5), a vector of damping parameters $\mathbf{R} \in \mathbb{R}^d$ is introduced, which must be chosen in δ_V, where $\delta_V = \overline{\delta}_P \cap \delta_X$.

Payoff	$\overline{\delta}_P$
Basket put	$\{\mathbf{R} \in \mathbb{R}^d,\ R_i > 0 \, \forall i \in \{1, \ldots, d\}\}$
Call on min	$\{\mathbf{R} \in \mathbb{R}^d,\ R_i < 0 \, \forall i \in \{1, \ldots, d\}, \sum_{i=1}^{d} R_i < -1\}$

Table 2.2: Strip of regularity, $\overline{\delta}_P$, of the conjugate of payoff transforms. Refer to [24, 34] for more details on the derivation.

Model	δ_X
GBM	$\mathbb{R}^d$
VG	$\{\mathbf{R} \in \mathbb{R}^d, \left(1 + \nu \langle \boldsymbol{\theta}, \mathbf{R} \rangle - \frac{1}{2} \nu \langle \mathbf{R}, \mathbf{\Sigma} \mathbf{R} \rangle\right) > 0\}$
NIG	$\{\mathbf{R} \in \mathbb{R}^d, \left(\alpha^2 - \langle (\boldsymbol{\beta} - \mathbf{R}), \mathbf{\Delta}(\boldsymbol{\beta} - \mathbf{R}) \rangle\right) > 0\}$

Table 2.3: Strip of analyticity, δ_X, of the characteristic functions for the different pricing models. Refer to [24] for further details.

Remark 2.1 (About the strip of regularity)**.** Compared to the 1D case, in the multivariate setting, the choice of the vector of damping parameters $\mathbf{R}$, which satisfies the analyticity condition in Table 2.3, is nontrivial requiring numerical approximations. Moreover, to obtain more intuition, for the multivariate NIG model with $\mathbf{\Delta} = \boldsymbol{I_d}$, the strip of regularity δ_X^{NIG} is an open ball centered at $\boldsymbol{\beta}$ with radius α. This fact further complicates the arbitrary choice for damping parameters when the integrand is anisotropic because we must first identify the spherical boundary to determine the admissible combinations of values for the damping parameters enforcing the integrability. In addition, the dimensionality affects the area of the strip of regularity because, for fixed $\alpha, \{\beta_i\}_{i=1}^{d}$, increasing the problem dimensionality shrinks the strip of regularity. To illustrate this, for $R_1 = \ldots = R_d, \beta_1 = \ldots = \beta_d$, we can easily obtain the strip of regularity in d dimensions as follows:

$$(R_1 - \beta_1)^2 < \left(\frac{\alpha}{\sqrt{d}}\right)^2. \tag{2.6}$$

Equation (2.6) demonstrates that increasing d shrinks the radius of the ball characterizing δ_X^{MNIG} in Table 2.3 by a factor of $\sqrt{d}$.

3 Methodology of our Approach

3.1 Characterization of the optimal damping rule

This section aims to motivate and propose a heuristic rule for the optimal choice of the damping parameters $\mathbf{R}$ that can accelerate the convergence of the numerical quadrature in the Fourier space when approximating (2.5) for pricing multi-asset options under the considered pricing models for various parameters. The main idea is to establish a connection between the damping parameter values, integrand properties, and quadrature error.

Before considering the integral of interest (2.5), we provide the general motivation for the rule through a simple 1D integration example for a real-valued function f w.r.t. a weight function $\lambda(\cdot)$ over the support interval $[a, b]$ (finite, half-infinite, or doubly infinite interval):

$$I(f) := \int_a^b f(x)\lambda(x)dx \approx \sum_{k=1}^{N} w_k f(x_k) := Q_N(f), \tag{3.1}$$

where the quadrature estimator, $Q_N(f)$ is characterized by the nodes $\{x_k\}_{k=1}^N$ which are the roots of the appropriate orthogonal polynomial, $\pi_k(x)$, and $\{w_k\}_{k=1}^N$ are the appropriate quadrature weights. Moreover, $\mathcal{E}_{Q_N}(f)$ denotes the quadrature error (remainder), defined as $\mathcal{E}_{Q_N}(f) := I(f) - Q_N(f)$.

The analysis of the quadrature error can be performed through two representations: the first relies on estimates based on high-order derivatives for a smooth function f [28, 20, 59]. These error representations are of limited practical value and use because high-order derivatives are usually challenging to estimate and control, particularly with relation to the damping parameters in this context as a complex rule for optimally choosing these parameters may result. For this reason, to derive our rule, we opt for the second form of quadrature error representation, valid for functions that can be extended holomorphically into the complex plane, which corresponds to the case in (2.5).

Several approaches exist for estimating the error $\mathcal{E}_{Q_N}(f)$ when f is holomorphic: (i) methods of contour integration [54, 22], (ii) methods based on Hilbert space norm estimates [19, 21] which consider $\mathcal{E}_{Q_N}$ as a linear functional on f, and (iii) methods based on the approximation theory [2, 56]. Independent of the approach, the results are often comparable because the error bounds involve the supremum norm of f.

We focus on error estimates based on contour integration tools to showcase these error bounds. This approach uses Cauchy's theorem in the theory of complex variables to express the value of an analytic function at some point z by means of a contour integral (Cauchy integral) extended over a simple closed curve (or open arc) in the complex plane encircling the point z. We assume that the function f can be analytically extended into a sizable region of the complex plane, containing the interval $[a, b]$ with no singularities. Then, we have the following result.

Theorem 3.1. *The error integral in the approximation* (3.1) *can be expressed as*

$$\mathcal{E}_{Q_N}(f) = \frac{1}{2\pi i}\oint_{\mathcal{C}} K_N(z)f(z)dz, \tag{3.2}$$

where

$$K_N(z) = \frac{H_N(z)}{\pi_N(z)}, \quad H_N(z) = \int_a^b \lambda(x)\frac{\pi_N(z)}{z-x}dx, \tag{3.3}$$

and $\mathcal{C}$ is a contour[3] *containing the interval $[a, b]$ within which $f(z)$ has no singularities.*

Proof. We refer to [22, 28] for proof of Theorem 3.1. ☐

[3] Two choices of $\mathcal{C}$ are most frequently made: $\mathcal{C} = \mathcal{C}_r$, the circle $|z| = r, r > 1$, and $C = \mathcal{C}_\rho$, the ellipse with foci at a and b, where the sum of its semiaxes is equal to $\rho, \rho > 1$. Circles can only be used if the analyticity domain is sufficiently large, and ellipses have the advantage of shrinking to the interval $[a, b]$ when $\rho \to 1$, making them suitable for dealing with functions that are analytic on the segment $[a, b]$.

In the finite case, the contour $\mathcal{C}$ is closed and (3.3) represents an analytic function in the connected domain $\mathbb{C} \setminus [a, b]$ while we may take $\mathcal{C}$ to lie on the upper and lower edges of the real axis in the infinite case for large $|x|$. Discussions on choosing adequate contours are found in [25, 22, 21]. Moreover, precise estimates of $H_n(z)$ were derived in [22, 26].

As $f(\cdot)$ has no singularities within $\mathcal{C}$, using Theorem 3.1, we obtain

$$|\mathcal{E}_{Q_N}(f)| \leq \frac{1}{2\pi} \sup_{z \in \mathcal{C}} |f(z)| \oint_{\mathcal{C}} |K_N(z)||dz|, \tag{3.4}$$

where the quantity $\oint_{\mathcal{C}} |K_n(z)||dz|$ depends only on the quadrature rule. We expect that when the size of the contour increases, $\oint_{\mathcal{C}} |K_n(z)||dz|$ decreases, whereas $\sup_{z \in \mathcal{C}} |f(z)|$ increases by the maximum modulus theorem. The optimal choice of the contour $\mathcal{C}$ is the one that minimizes the right-handside of (3.4).

Extending the error bound (3.4) to the multidimensional setting can be performed straightforwardly using tensorization tools. Moreover, the dependence of the upper bound on $\sup_{z \in \mathcal{C}} |f(z)|$ is independent of the quadrature method. Therefore, motivated by the error bound (3.4), we propose a heuristic rule for choosing the damping parameters that improves the numerical convergence of the designed numerical quadrature method (see Section 3.2) when approximating (2.5). The rule consists in solving the following constrained optimization problem

$$\mathbf{R}^* := \mathbf{R}^*(\mathbf{\Theta}_m, \mathbf{\Theta}_p) = \underset{\mathbf{R} \in \delta_V}{\arg\min} \, \|g(\mathbf{u}; \mathbf{R}, \mathbf{\Theta}_m, \mathbf{\Theta}_p)\|_\infty, \tag{3.5}$$

where $\mathbf{R}^* := (R_1^*, \ldots, R_d^*)$ denotes the optimal damping parameters.

In our setting, the integrand defined in Equation (2.5) attains its maximum at the origin point $\mathbf{u} = \mathbf{0}_{\mathbb{R}^d}$; thus solving (3.5) is reduced to a simpler optimization problem given by (3.6)

$$\mathbf{R}^* = \underset{\mathbf{R} \in \delta_V}{\arg\min} \, g(\mathbf{0}_{\mathbb{R}^d}; \mathbf{R}, \mathbf{\Theta}_m, \mathbf{\Theta}_p). \tag{3.6}$$

Equation (3.6) cannot be solved analytically, especially in high dimensions; therefore, we solve it numerically, approximating $\mathbf{R}^*$ by $\overline{\mathbf{R}} = (\overline{R}_1, \ldots, \overline{R}_d)$. In this context, we used the interior point method [11, 12] with an accuracy of order 10^{-6}.

The numerical investigation through different models and parameters (for illustration, we refer to Figure 3.1 for the single put option under the different models, and Figure 3.2 for the 2D-Basket put under VG) confirmed that the damping parameters have a considerable effect on the properties of the integrand, particularly its peak, tail-heaviness, and oscillatory behavior. We observed that the damping parameters that produce the lowest peak of the integrand around the origin are associated with a faster convergence of the relative quadrature error than other damping parameters. Moreover, we observed that highly peaked integrands are more likely to oscillate, implying a deteriorated convergence of the numerical quadrature. Independent of the quadrature methods explained in Section 3.2, this observation was consistent for several parameter constellations under the three tested pricing dynamics, GBM, VG, and NIG, and for different dimensions of the basket put and rainbow options. Section 4.1.2 illustrates the computational advantage of the optimal damping rule on the error convergence for the multi-asset basket put and call on min options under different models.

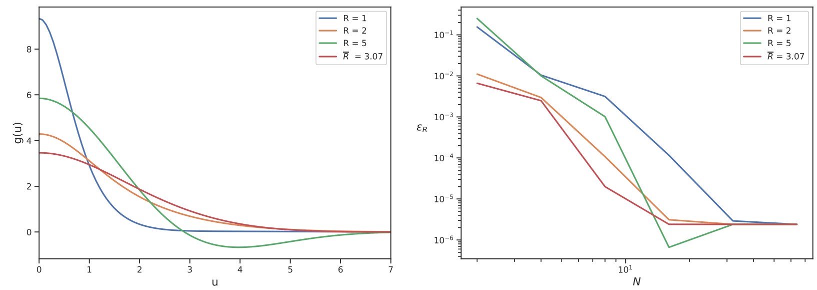

(a) $S_0 = 100, K = 100, r = 0\%, T = 1, \sigma = 0.4$

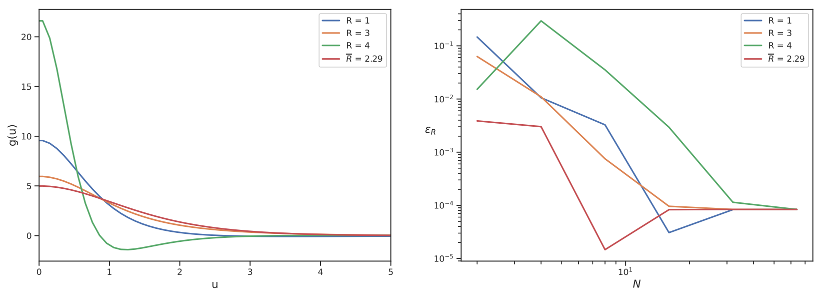

(b) $S_0 = 100, K = 100, r = 0\%, T = 1, \sigma = 0.4, \theta = -0.3, \nu = 0.257$

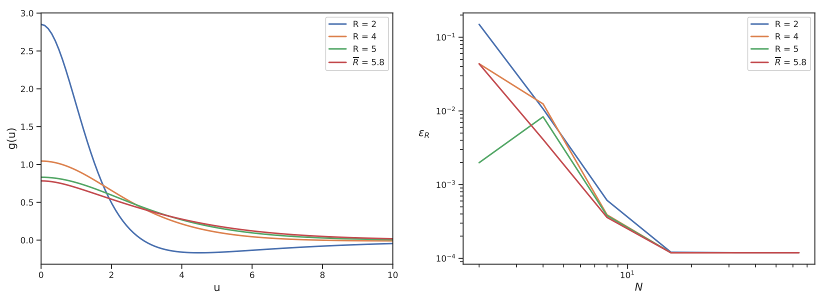

(c) $S_0 = 100, K = 100, r = 0\%, T = 1, \alpha = 10, \beta = -3, \delta = 0.2$

Figure 3.1: 1D illustration: (Left) Shape of the integrand w.r.t the damping parameter, R. (Right) $\mathcal{E}_R$ convergence w.r.t. N, using Gauss–Laguerre quadrature for the European put option under (a) GBM, (b) VG, and (c) NIG pricing models. The relative quadrature error $\mathcal{E}_R$ is defined as $\mathcal{E}_R = \frac{|Q_N[g] - \text{Reference Value}|}{\text{Reference Value}}$, where Q_N is the quadrature estimator of (2.5) based on the Gauss–Laguerre rule.

Remark 3.2. The d-dimensional optimization problem (3.6) is simplified further to a 1D problem when the integrand is isotropic.

Remark 3.3. Other rules for choosing the damping parameters can be investigated to improve the numerical convergence of quadrature methods. One can account for additional features, such as (i) the distance of the damping parameters to the poles, which affects the choice of the integration

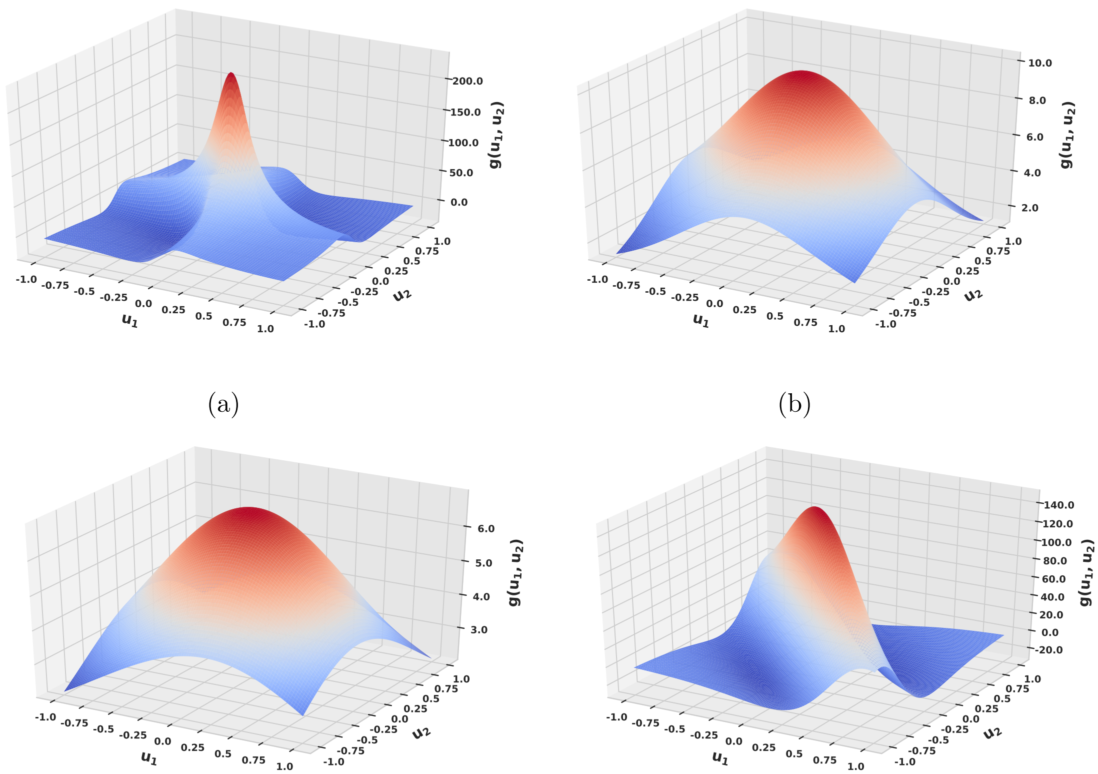

(a) (b)

(c) (d)

Figure 3.2: Effect of the damping parameters on the shape of the integrand in the case of 2D-basket put option under the VG model with parameters $\boldsymbol{\sigma} = (0.4, 0.4)$, $\boldsymbol{\theta} = (-0.3, -0.3), \nu = 0.257$. (a) $\mathbf{R} = (0.2, 0.2)$ (b) $\mathbf{R} = (1, 1)$, (c) $\mathbf{R} = (2, 2)$, (d) $\mathbf{R} = (3, 3)$.

contour in (3.2), or (ii) controlling the regularity of the integrand via high-order derivative estimates. However, we expect such rules to be more complicated and computationally expensive (e.g., the evaluation of the gradient of the integrand). Investigating other rules remains for future work.

3.2 Numerical evaluation of the inverse Fourier integrals using hierarchical deterministic quadrature methods

We aim to approximate (2.5) efficiently using a tensorization of quadrature formulas over $\mathbb{R}^d$. When using Fourier transforms for option pricing, the standard numerical approach truncates and discretizes the integration domain and uses FFT based on bounded quadrature formulas, such as the trapezoidal rule. This option is efficient in the 1D setting, as the estimation of the truncation intervals based, for instance, on the cumulants, was widely covered in the literature. It remains affordable even though the additional cost might be high due to the inappropriate choice of truncation parameters. However, this is not the case in the multidimensional setting because determining the truncation parameters becomes more challenging. Moreover, the truncation errors nontrivially depend on the damping parameter values. Choosing larger than necessary truncation domains leads to a more significant increase in the computational effort for higher dimensions.

For this reason, we use the DI approach with Gaussian quadrature rules. Moreover, our numerical investigation (see Appendix B) suggests that Gauss–Laguerre quadrature exhibits faster convergence than the Gauss–Hermite rule. Therefore, we used Laguerre quadrature on semi-infinite domains after applying the necessary transformations.

Before defining the multivariate quadrature estimators, we first introduce the notation in the univariate setting (For more details see [15]). In addition, β denotes a non-negative integer, referred to as the "discretization level," and $m : \mathbb{N} \to \mathbb{N}$ represents a strictly increasing function with $m(0) = 0$ and $m(1) = 1$, called a "level-to-nodes function." At each level β, we consider a set of $m(\beta)$ distinct quadrature points $\mathcal{H}^{m(\beta)} = \left\{x_\beta^1, x_\beta^2, \ldots, x_\beta^{m(\beta)}\right\} \subset \mathbb{R}$, and a set of quadrature weights, $\boldsymbol{\omega}^{m(\beta)} = \left\{\omega_\beta^1, \omega_\beta^2, \ldots, \omega_\beta^{m(\beta)}\right\}$. We also let $C^0(\mathbb{R})$ be the space of real-valued continuous functions over $\mathbb{R}$. We define the univariate quadrature operator applied to a function $f \in C^0(\mathbb{R})$ as follows:

$$Q^{m(\beta)} : C^0(\mathbb{R}) \to \mathbb{R}, \quad Q^{m(\beta)}[f] := \sum_{j=1}^{m(\beta)} f\left(x_\beta^j\right) \omega_\beta^j .$$

In our case, in (2.5), we have a multivariate integration problem of g over $\mathbb{R}^d$. Accordingly, for a multi-index $\boldsymbol{\beta} = (\beta_i)_{i=1}^d \in \mathbb{N}^d$, the d-dimensional quadrature operator applied to g is defined as[4]

$$Q^{m(\boldsymbol{\beta})} : C^0\left(\mathbb{R}^d\right) \to \mathbb{R}, \quad Q^{m(\boldsymbol{\beta})} = \bigotimes_{i=1}^d Q^{m(\beta_i)},$$

$$Q_d^{m(\boldsymbol{\beta})}[g] = \sum_{j=1}^{\#\mathcal{T}^{m(\boldsymbol{\beta})}} g\left(\widehat{x}_j\right) \overline{\omega}_j,$$

where $\widehat{x}_j \in \mathcal{T}^{m(\boldsymbol{\beta})} := \prod_{i=1}^d \mathcal{H}^{m(\beta_i)}$ (with cardinality $\#\mathcal{T}^{m(\boldsymbol{\beta})} = \prod_{i=1}^d m\left(\beta_i\right)$ and $m(\beta_i) = N_i$ quadrature points in the dimension of x_i), and $\overline{\omega}_j$ is a product of the weights of the univariate quadrature rule. To simplify the notation, we replace $Q_d^{m(\boldsymbol{\beta})}$ with $Q_d^{\boldsymbol{\beta}}$.

We define the set of differences $\Delta Q_d^{\boldsymbol{\beta}}$ for indices $i \in \{1, \ldots, d\}$ as follows:

$$\Delta_i Q_d^{\boldsymbol{\beta}} := \begin{cases} Q_d^{\boldsymbol{\beta}} - Q_d^{\boldsymbol{\beta}'}, \text{ with } \boldsymbol{\beta}' = \boldsymbol{\beta} - \mathbf{e}_i, \text{ when } \beta_i > 0, \\ Q_d^{\boldsymbol{\beta}}, \quad \text{otherwise,} \end{cases} \tag{3.7}$$

where $\mathbf{e}_i$ denotes the ith d-dimensional unit vector. Then, using the telescopic property, the quadrature estimator, defined w.r.t. a choice of the set of multi-indices $\mathcal{I} \subset \mathbb{N}^d$, is expressed by[5, 6]

$$Q_d^{\mathcal{I}} = \sum_{\boldsymbol{\beta} \in \mathcal{I}} \Delta Q_d^{\boldsymbol{\beta}}, \quad \text{with } \Delta Q_d^{\boldsymbol{\beta}} = \left(\bigotimes_{i=1}^d \Delta_i\right) Q_d^{\boldsymbol{\beta}}, \tag{3.8}$$

[4]The n-th quadrature operator acts only on the n-th variable of g.

[5]For instance, when $d = 2$, then $\Delta Q_2^{\boldsymbol{\beta}} = \Delta_2 \Delta_1 Q_2^{(\beta_1,\beta_2)} = Q_2^{(\beta_1,\beta_2)} - Q_2^{(\beta_1,\beta_2-1)} - Q_2^{(\beta_1-1,\beta_2)} + Q_2^{(\beta_1-1,\beta_2-1)}$.

[6]To ensure the validity of the telescoping sum expansion, the index set $\mathcal{I}$ must satisfy the admissibility condition (*i.e.*, $\boldsymbol{\beta} \in \mathcal{I}, \boldsymbol{\alpha} \le \boldsymbol{\beta} \Rightarrow \boldsymbol{\alpha} \in \mathcal{I}$, where $\boldsymbol{\alpha} \le \boldsymbol{\beta}$ is defined as $\alpha_i \le \beta_i, i = 1, \ldots, d$).

and the quadrature error can be written as

$$\mathcal{E}_Q = \left|Q_d^{\infty}[g] - Q_d^{\mathcal{I}}[g]\right| \leq \sum_{\boldsymbol{\beta} \in \mathbb{N}^d \setminus \{\mathcal{I}\}} \left|\Delta Q_d^{\boldsymbol{\beta}}[g]\right|, \tag{3.9}$$

where

$$Q_d^{\infty} := \sum_{\beta_1=0}^{\infty} \cdots \sum_{\beta_d=0}^{\infty} \Delta Q_d^{(\beta_1,\ldots,\beta_d)} = \sum_{\boldsymbol{\beta} \in \mathbb{N}^d} \Delta Q_d^{\boldsymbol{\beta}}.$$

In Equation (3.8), the choice of (i) the strategy for the construction of the index set $\mathcal{I}$ and (ii) the hierarchy of quadrature points determined by $m(\cdot)$ defines different hierarchical quadrature methods. Table 3.1 presents the details of the methods considered in this work.

Quadrature Method	$m(\cdot)$	$\mathcal{I}$
Tensor Product (TP)	$m(\beta) = \beta$	$\mathcal{I}^{\text{TP}}(l) = \{\boldsymbol{\beta} \in \mathbb{N}^d : \ \max_{1 \leq i \leq d}(\beta_i - 1) \leq l\}$
Smolyak (SM) Sparse Grids	$m(\beta) = 2^{\beta-1}+1,\ \beta > 1, m(1) = 1$	$\mathcal{I}^{\text{SM}}(l) = \{\boldsymbol{\beta} \in \mathbb{N}^d : \ \sum_{1 \leq i \leq d}(\beta_i - 1) \leq l\}$
Adaptive Sparse Grid Quadrature (ASGQ)	$m(\beta) = 2^{\beta-1}+1,\ \beta > 1, m(1) = 1$	$\mathcal{I}^{\text{ASGQ}} = \{\boldsymbol{\beta} \in \mathbb{N}_+^d : P_{\boldsymbol{\beta}} \geq \overline{T}\}$ (see (3.10) and (3.11))

Table 3.1: Construction details for the quadrature methods. $l \in \mathbb{N}$ represents a given level. $\overline{T} \in \mathbb{R}$ is a threshold value.

In many situations, the tensor product (TP) estimator can become rapidly unaffordable because the number of function evaluations increases exponentially with the problem dimensionality, known as the *curse of dimensionality*. We use Smolyak (SM) and ASGQ methods based on sparsification and dimension-adaptivity techniques to overcome this issue. For both TP and SM methods, the construction of the index set is performed a priori. However, ASGQ allows for the a posteriori and adaptive construction of the index set $\mathcal{I}$ by greedily exploiting the mixed regularity of the integrand during the actual computation of the quantity of interest. The construction of $\mathcal{I}^{\text{ASGQ}}$ is performed through profit thresholding, where new indices are selected iteratively based on the error versus cost-profit rule, with a hierarchical surplus defined by

$$P_{\boldsymbol{\beta}} = \frac{|\Delta E_{\boldsymbol{\beta}}|}{\Delta \mathcal{W}_{\boldsymbol{\beta}}}, \tag{3.10}$$

where $\Delta \mathcal{W}_{\boldsymbol{\beta}}$ is the work contribution (*i.e.*, the computational cost required to add $\Delta Q_d^{\boldsymbol{\beta}}$ to $Q_d^{\mathcal{I}^{\text{ASGQ}}}$) and $\Delta E_{\boldsymbol{\beta}}$ is the error contribution (*i.e.*, a measure of how much the quadrature error would decrease once $\Delta Q_d^{\boldsymbol{\beta}}$ has been added to $Q_d^{\mathcal{I}^{\text{ASGQ}}}$):

$$\begin{aligned} \Delta E_{\boldsymbol{\beta}} &= \left|Q_d^{\mathcal{I}^{\text{ASGQ}} \cup \{\boldsymbol{\beta}\}}[g] - Q_d^{\mathcal{I}^{\text{ASGQ}}}[g]\right| \\ \Delta \mathcal{W}_{\boldsymbol{\beta}} &= \text{Work}\left[Q_d^{\mathcal{I}^{\text{ASGQ}} \cup \{\boldsymbol{\beta}\}}[g]\right] - \text{Work}\left[Q_d^{\mathcal{I}^{\text{ASGQ}}}[g]\right]. \end{aligned} \tag{3.11}$$

The convergence speed for all quadrature methods in this work is determined by the behavior of the quadrature error defined in (3.9). In this context, given the model and option parameters, the convergence rate depends on the damping parameter values, which control the regularity of the integrand g in the Fourier space (see (2.5)).

We let $N := \prod_{i=1}^{d} m(\beta_i)$ denote the total number of quadrature points used by each method. For the TP method, we have the following [20]:

$$\mathcal{E}_Q^{\mathrm{TP}}(N; \mathbf{R}) = \mathcal{O}\left(N^{-\frac{r_t}{d}}\right) \tag{3.12}$$

for functions with bounded total derivatives up to order $r_t := r_t(\mathbf{R})$. When using SM sparse grids (not adaptive), we obtain the following [53, 58, 29, 4]:

$$\mathcal{E}_Q^{\mathrm{SM}}(N; \mathbf{R}) = \mathcal{O}\left(N^{-r_m}(\log N)^{(d-1)(r_m)+1)}\right) \tag{3.13}$$

for functions with bounded mixed partial derivatives up to order $r_m := r_m(\mathbf{R})$. Moreover, it was observed in [30] that the convergence is even spectral for analytic functions ($r_m \to +\infty$). For the ASGQ method, we achieve [15]

$$\mathcal{E}_Q^{\mathrm{ASGQ}}(N; \mathbf{R}) = \mathcal{O}\left(N^{-r_w/2}\right) \tag{3.14}$$

where r_w is related to the degree of weighted mixed regularity of the integrand.

In (3.12), (3.13), and (3.14), we emphasize the dependence of the convergence rates on the damping parameters $\mathbf{R}$, which is only valid in this context because these parameters control the regularity of the integrand in the Fourier space. Moreover, our optimized choice of $\mathbf{R}$ is not only used to increase the number of derivatives but also to reduce the bounds on these derivatives.

4 Numerical Experiments and Results

In this section, we present the results of different numerical experiments conducted for pricing multi-asset European basket and rainbow options with the respective payoffs:

$$(i)\ P(\mathbf{X}_T; K) = \max\left(K - \frac{1}{d}\sum_{i=1}^{d} e^{X_T^i}, 0\right); \quad (ii)\ P(\mathbf{X}_T; K) = \max\left(\min\left(e^{X_T^1}, \ldots, e^{X_T^d}\right) - K, 0\right).$$

These examples are tested under the multivariate (i) GBM, (ii) VG and (iii) NIG models with various parameter constellations for different dimensions $d \in \{2, 4, 6\}$. The tested model parameters are justified from the literature on model calibration [37, 57, 16, 9, 1, 33]. The detailed illustrated examples are presented in Tables 4.1, 4.2, and 4.3. To compare the methods in this work, we consider relative errors normalized by the reference prices. The error is the relative quadrature error defined as $\mathcal{E}_R = \frac{|Q_d^{\mathcal{I}}[g] - \text{Reference Value}|}{\text{Reference Value}}$ when using quadrature methods, and the 95% relative statistical error of the MC method is estimated by the virtue of the central limit theorem (CLT) as

$$\mathcal{E}_R \approx \frac{C_\alpha \times \sigma_M}{\text{Reference Value} \times \sqrt{M}} \tag{4.1}$$

where $C_\alpha = 1.96$ for 95% confidence level, M is the number of MC samples, and σ_M is the standard deviation of the quantity of interest.

The numerical results were obtained using a cluster machine with the following characteristics: clock speed 2.1 GHw, #CPU cores: 72, and memory per node 256 GB. Furthermore, the computer code is written in the MATLAB (version R2021b). The ASGQ implementation was based on `https://sites.google.com/view/sparse-grids-kit` (For more details on the implementation we refer to [48]).

Through various tested examples, in section 4.1.1, we demonstrate the importance of sparsification and adaptivity in the Fourier space for accelerating quadrature convergence. Moreover, in section 4.1.2 , we reveal the importance of the choice of the damping parameters on the numerical complexity of the used quadrature methods. Finally, in Section 4.2, we illustrate that our approach achieves substantial computational gains over the MC method for different dimensions and parameter constellations to meet a certain relative error tolerance (of practical interest) that we set to be sufficiently small.

Example	**Option**	**Parameters**	**Reference Value** (95% Statistical Error)	**Optimal damping parameters** $\overline{\mathbf{R}}$
Example 1	2D-Basket put	$\boldsymbol{\sigma} = (0.4, 0.4), \mathbf{C} = I_2, K = 100$	11.4474 ($8e^{-04}$)	$(2.5, 2.5)$
Example 2	2D-Basket put	$\boldsymbol{\sigma} = (0.4, 0.8), \mathbf{C} = I_2, K = 100$	17.831 ($1.2e^{-03}$)	$(2.1, 1.2)$
Example 3	2D-Call on min	$\boldsymbol{\sigma} = (0.4, 0.4), \mathbf{C} = I_2, K = 100$	3.4603 ($6e^{-04}$)	$(-3.4, -3.4)$
Example 4	2D-Call on min	$\boldsymbol{\sigma} = (0.4, 0.8), \mathbf{C} = I_2, K = 100$	3.7411 ($8.2e^{-04}$)	$(-3.6, -1.8)$
Example 5	4D-Basket put	$\boldsymbol{\sigma} = (0.4, 0.4, 0.4, 0.4)$, $\mathbf{C} = I_4, K = 100$	8.193 ($6e^{-04}$)	$(2.1, 2.1, 2.1, 2.1)$
Example 6	4D-Basket put	$\boldsymbol{\sigma} = (0.2, 0.4, 0.6, 0.8)$, $\mathbf{C} = I_4, K = 100$	11.3014 ($8e^{-04}$)	$(2.4, 1.9, 1.5, 1.2)$
Example 7	4D-Call on min	$\boldsymbol{\sigma} = (0.4, 0.4, 0.4, 0.4)$, $\mathbf{C} = I_4, K = 100$	0.317 ($2e^{-04}$)	$(-3.1, -3.1, -3.1, -3.1)$
Example 8	4D-Call on min	$\boldsymbol{\sigma} = (0.2, 0.4, 0.6, 0.8)$, $\mathbf{C} = I_4, K = 100$	0.2382 ($1e^{-04}$)	$(-6.4, -3.1, -2.1, -1.6)$
Example 9	6D-Basket put	$\boldsymbol{\sigma} = (0.4, 0.4, 0.4, 0.4, 0.4, 0.4)$, $\mathbf{C} = I_6, K = 60$	0.0041 ($8.8e^{-06}$)	$(2.0, 2.0, 2.0, 2.0, 2.0, 2.0)$
Example 10	6D-Basket put	$\boldsymbol{\sigma} = (0.2, 0.3, 0.4, 0.5, 0.6, 0.7)$, $\mathbf{C} = I_6, K = 60$	0.012702 ($1.8e^{-05}$)	$(2.3, 2.1, 1.9, 1.7, 1.5, 1.3)$
Example 11	6D-Call on min	$\boldsymbol{\sigma} = (0.4, 0.4, 0.4, 0.4, 0.4, 0.4)$, $\mathbf{C} = I_6, K = 100$	0.038 ($4.4e^{-05}$)	$(-3.0, -3.0, -3.0, -3.0, -3.0, -3.0)$
Example 12	6D-Call on min	$\boldsymbol{\sigma} = (0.2, 0.3, 0.4, 0.5, 0, 6, 0.7)$, $\mathbf{C} = I_6, K = 100$	0.0301 ($3.7e^{-05}$)	$(-6.0, -3.9, -3.0, -2.4, -2.0, -1.8)$

Table 4.1: Examples of multi-asset options under the multivariate GBM model. In all examples, $S_0^i = 100, i = 1, \ldots, d, T = 1, r = 0$. Reference values are computed with MC using 10^9 samples, with 95% statistical error estimates reported between parentheses. $\overline{R}$ is rounded to one decimal place.

Example	Option	Parameters	Reference Value (95% Statistical Error)	Optimal damping parameters $\overline{\mathbf{R}}$
Example 13	2D-Basket put	$\boldsymbol{\sigma} = (0.4, 0.4)$,$\boldsymbol{\theta} = (-0.3, -0.3)$, $\nu = 0.257, K = 100$	11.7589 $(1e^{-03})$	$(1.7, 1.7)$
Example 14	2D-Basket put	$\boldsymbol{\sigma} = (0.4, 0.8)$,$\boldsymbol{\theta} = (-0.3, 0)$, $\nu = 0.257, K = 100$	17.6688 $(1.2e^{-03})$	$(1.7, 1.0)$
Example 15	2D-Call on min	$\boldsymbol{\sigma} = (0.4, 0.4)$,$\boldsymbol{\theta} = (-0.3, -0.3)$, $\nu = 0.257, K = 100$	3.9601 $(7e^{-04})$	$(-3.5, -3.5)$
Example 16	2D-Call on min	$\boldsymbol{\sigma} = (0.4, 0.8)$,$\boldsymbol{\theta} = (-0.3, 0)$, $\nu = 0.257, K = 100$	3.3422 $(8e^{-04})$	$(-4.0, -3.5)$
Example 17	4D-Basket put	$\boldsymbol{\sigma} = (0.4, 0.4, 0.4, 0.4)$, $\boldsymbol{\theta} = (-0.3, -0.3, -0.3, -0.3)$, $\nu = 0.257, K = 100$	8.9441 $(8e^{-04})$	$(1.2, 1.2, 1.2, 1.2)$
Example 18	4D-Basket put	$\boldsymbol{\sigma} = (0.2, 0.4, 0.6, 0.8)$, $\boldsymbol{\theta} = (-0.3, -0.2, -0.1, 0)$, $\nu = 0.257, K = 100$	11.2277 $(8e^{-04})$	$(1.6, 1.4, 1.1, 0.9)$
Example 19	4D-Call on min	$\boldsymbol{\sigma} = (0.4, 0.4, 0.4, 0.4)$, $\boldsymbol{\theta} = (-0.3, -0.3, -0.3, -0.3)$, $\nu = 0.257, K = 100$	0.6137 $(2e^{-04})$	$(-3.2, -3.2, -3.2, -3.2)$
Example 20	4D-Call on min	$\boldsymbol{\sigma} = (0.2, 0.4, 0.6, 0.8)$, $\boldsymbol{\theta} = (-0.3, -0.2, -0.1, 0)$, $\nu = 0.257, K = 100$	0.2384 $(1e^{-04})$	$(-6.6, -3.0, -2.0, -1.5)$
Example 21	6D-Basket put	$\boldsymbol{\sigma} = (0.4, 0.4, 0.4, 0.4, 0.4, 0.4)$, $\boldsymbol{\theta} = -(0.3, 0.3, 0.3, 0.3, 0.3, 0.3)$, $\nu = 0.257, K = 60$	0.1691 $(1e^{-06})$	$(1.1, 1.1, 1.1, 1.1, 1.1, 1.1)$
Example 22	6D-Basket put	$\boldsymbol{\sigma} = (0.2, 0.3, 0.4, 0.5, 0.6, 0.7)$, $\boldsymbol{\theta} = (-0.3, -0.2, -0.1, 0, 0.1, 0.2)$, $\nu = 0.257, K = 60$	0.04634 $(5e^{-05})$	$(2.1, 1.9, 1.7, 1.6, 1.4, 1.2)$
Example 23	6D-Call on min	$\boldsymbol{\sigma} = (0.4, 0.4, 0.4, 0.4, 0.4, 0.4)$, $\boldsymbol{\theta} = -(0.3, 0.3, 0.3, 0.3, 0.3, 0.3)$, $\nu = 0.257, K = 100$	0.16248 $(1e^{-04})$	$(-3.1, -3.1, -3.1, -3.1, -3.1, -3.1)$
Example 24	6D-Call on min	$\boldsymbol{\sigma} = (0.2, 0.3, 0.4, 0.5, 0.6, 0.7)$, $\boldsymbol{\theta} = (-0.3, -0.2, -0.1, 0, 0.1, 0.2)$, $\nu = 0.257, K = 100$	0.02269 $(4e^{-05})$	$(-6.5, -3.7, -2.6, -2.0, -1.7, -1.4)$

Table 4.2: Examples of multi-asset options under the multivariate VG model. In all examples, $S_0^i = 100, i = 1, \ldots, d, T = 1, r = 0$. Reference values are computed with MC using 10^9 samples, with 95% statistical error estimates reported between parentheses. $\overline{R}$ is rounded to one decimal place.

4.1 Combining the optimal damping heuristic rule with hierarchical deterministic quadrature methods

4.1.1 Effect of sparsification and dimension-adaptivity

In this section, we analyze the effect of dimension adaptivity and sparsification on the acceleration of the convergence of the relative quadrature error, $\mathcal{E}_R$. We elaborate a comparison between the TP, SM, and ASGQ methods when optimal damping parameters are used. Table 4.4 summarizes these

Example	Option	Parameters	Reference Value (95% Statistical Error)	Optimal damping parameters $\overline{\mathbf{R}}$
Example 25	2D-Basket put	$\boldsymbol{\beta} = (-3, -3), \alpha = 15$, $\delta = 0.2, \boldsymbol{\Delta} = \boldsymbol{I_2}, K = 100$	3.3199 $(3e^{-04})$	$(6.1, 6.1)$
Example 26	2D-Basket put	$\boldsymbol{\beta} = (-3, 0), \alpha = 10$, $\delta = 0.2, \boldsymbol{\Delta} = \boldsymbol{I_2}, K = 100$	3.8978 $(4e^{-04})$	$(4.6, 4.8)$
Example 27	2D-Call on min	$\boldsymbol{\beta} = (-3, -3), \alpha = 15$, $\delta = 0.2, \boldsymbol{\Delta} = \boldsymbol{I_2}, K = 100$	1.2635 $(2e^{-04})$	$(-9.9, -9.9)$
Example 28	2D-Call on min	$\boldsymbol{\beta} = (-3, 0), \alpha = 10$, $\delta = 0.2, \boldsymbol{\Delta} = \boldsymbol{I_2}, K = 100$	1.4476 $(2e^{-04})$	$(-7.5, -6.8)$
Example 29	4D-Basket put	$\boldsymbol{\beta} = (-3, -3, -3, -3), \alpha = 15$, $\delta = 0.4, \boldsymbol{\Delta} = \boldsymbol{I_4}, K = 100$	2.554 $(3e^{-04})$	$(4.0, 4.0, 4.0, 4.0)$
Example 30	4D-Basket put	$\boldsymbol{\beta} = (-3, -2, -1, 0), \alpha = 15$, $\delta = 0.4, \boldsymbol{\Delta} = \boldsymbol{I_4}, K = 100$	3.307 $(3e^{-04})$	$(4.0, 4.2, 4.2, 4.2)$
Example 31	4D-Call on min	$\boldsymbol{\beta} = (-3, -3, -3, -3), \alpha = 15$, $\delta = 0.4, \boldsymbol{\Delta} = \boldsymbol{I_4}, K = 100$	0.17374 $(5e^{-05})$	$(-8.8, -8.8, -8.8, -8.8)$
Example 32	4D-Call on min	$\boldsymbol{\beta} = (-3, -2, -1, 0), \alpha = 15$, $\delta = 0.4, \boldsymbol{\Delta} = \boldsymbol{I_4}, K = 100$	0.20327 $(7e^{-05})$	$(-6.5, -6.4, -6.3, -6.2)$
Example 33	6D-Basket put	$\boldsymbol{\beta} = (-3, -3, -3, -3, -3, -3)$, $\alpha = 15, \delta = 0.2, \boldsymbol{\Delta} = \boldsymbol{I_6}, K = 80$	0.01039 $(2e^{-05})$	$(3.1, 3.1, 3.1, 3.1, 3.1, 3.1)$
Example 34	6D-Basket put	$\boldsymbol{\beta} = (-3, -2, -1, 0, 1, 2)$, $\alpha = 15, \delta = 0.2, \boldsymbol{\Delta} = \boldsymbol{I_6}, K = 80$	$4.39e^{-04}$ $(3e^{-06})$	$(4.5, 4.6, 4.7, 4.8, 4.8, 4.9)$
Example 35	6D-Call on min	$\boldsymbol{\beta} = (-3, -3, -3, -3, -3, -3)$, $\alpha = 15, \delta = 0.2, \boldsymbol{\Delta} = \boldsymbol{I_6}, K = 110$	$6.034e^{-05}$ $(4e^{-06})$	$(-4.0, -4.0, -4.0, -4.0, -4.0, -4.0)$
Example 36	6D-Call on min	$\boldsymbol{\beta} = (-3, -2, -1, 0, 1, 2), \alpha = 15$, $\delta = 0.2, \boldsymbol{\Delta} = \boldsymbol{I_6}, K = 110$	$1.572e^{-04}$ $(2e^{-06})$	$(-3.2, -3.2, -3.1, -3.2, -3.2, -3.2)$

Table 4.3: Examples of multi-asset options under the multivariate NIG model. In all examples, $S_0^i = 100, i = 1, \ldots, d, T = 1, r = 0$. Reference values are computed with MC using 10^9 samples, with 95% statistical error estimates reported between parentheses. $\overline{R}$ is rounded to one decimal place.

findings. Through the numerical experiments, ASGQ consistently outperformed SM. Moreover, for the 2D options, the performance of the ASGQ and TP methods is model-dependent, with ASGQ being the best method for options under the GBM model. For $d = 4$, for options under the GBM and VG models, ASGQ performs better than TP, which is not the case for options under the NIG model. As for 6D options, ASGQ performs better than TP in most cases. These observations confirm that the effect of adaptivity and sparsification becomes more important as the dimension of the option increases. For the sake of illustration, Figure 4.1 compares ASGQ and TP for 4D options with anisotropic parameter sets under different pricing models when optimal damping parameters are used. Figure 4.1a reveals that, for the 4D-basket put option under the GBM model, the ASGQ method achieves $\mathcal{E}_{\mathcal{R}}$ below 1% using 13.3% of the work of the TP quadrature. Moreover, Figure 4.1c indicates that, for the 4D-basket put option under the VG model, the ASGQ method achieves $\mathcal{E}_{\mathcal{R}}$ below 0.1% using 25% of the work of the TP quadrature. In contrast, for the 4D-basket put option under the NIG model, Figure 4.1e reveals that the TP quadrature attains $\mathcal{E}_{\mathcal{R}}$ below 0.1%

using 10% of the work of the ASGQ.

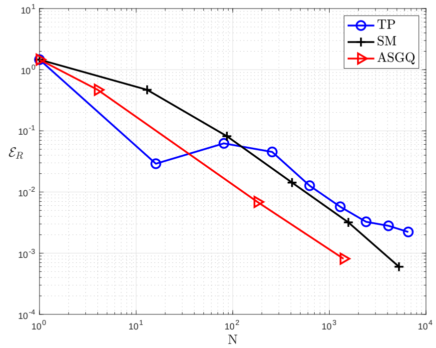

(a) Example 6 in Table 4.1

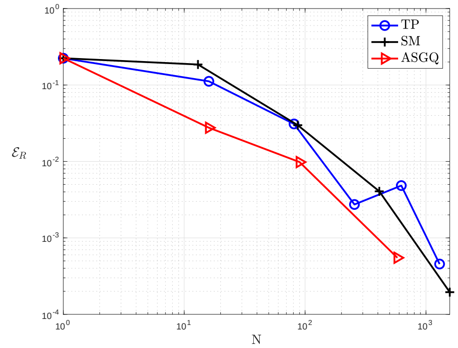

(b) Example 8 in Table 4.1

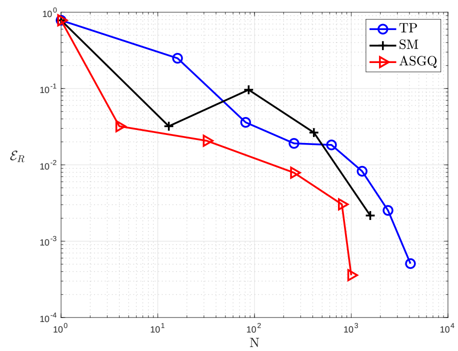

(c) Example 18 in Table 4.2

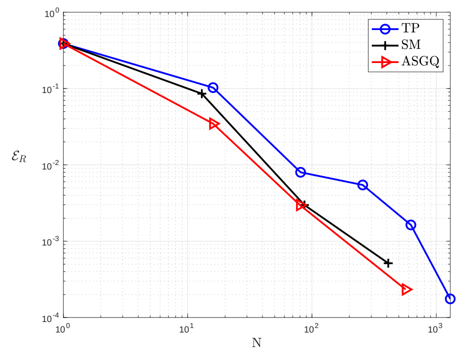

(d) Example 20 in Table 4.2

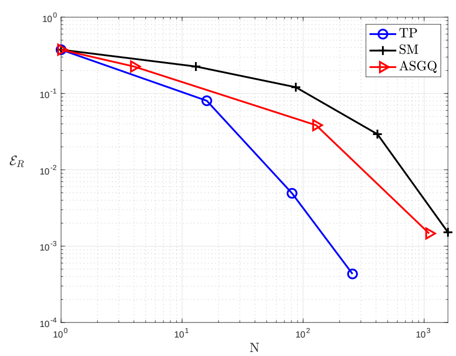

(e) Example 30 in Table 4.3

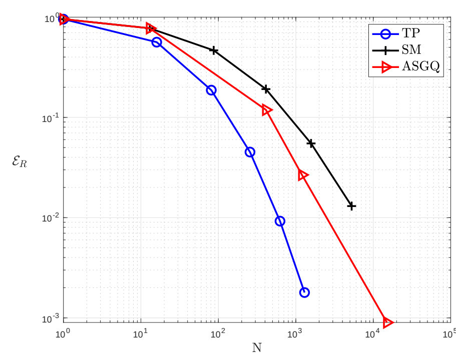

(f) Example 32 in Table 4.3

Figure 4.1: Convergence of the relative quadrature error, $\mathcal{E}_R$, w.r.t. N for TP, SM and ASGQ methods for European 4-asset options under GBM ((a) and (b)), VG ((c) and (d)), and NIG ((e) and (f)) models, when optimal damping parameters, $\overline{\mathbf{R}}$, are used.

4.1.2 Effect of the optimal damping rule

In this section, we present the computational benefit of using the optimal damping rule proposed in Section 3.1 on the convergence speed of the relative quadrature error of various methods when pricing the multi-asset European basket and rainbow options. Figures 4.2, 4.3, and 4.4 illustrate that the optimal damping parameters lead to substantially better error convergence behavior. For instance, Figure 4.2a reveals that, for the 4D-basket put option under the GBM model, ASGQ achieves $\mathcal{E}_{\mathcal{R}}$ below 0.1% using around $N = 1500$ quadrature points when using optimal damping parameters, compared to around $N = 5000$ points to achieve a similar accuracy for damping parameters shifted by $+1$ in each direction w.r.t. the optimal values. When using damping parameters shifted by $+2$ in each direction w.r.t. the optimal values, we do not reach $\mathcal{E}_{\mathcal{R}} = 10\%$, even using $N = 5000$ quadrature points. Similarly, for the 4D-call on min option under the VG model, Figure 4.3b illustrates that ASGQ achieves $\mathcal{E}_{\mathcal{R}}$ below 0.1% using around $N = 500$ quadrature points when using the optimal damping parameters. In contrast, ASGQ cannot achieve $\mathcal{E}_{\mathcal{R}}$ below 1% when using damping parameters shifted by -1 in each direction w.r.t. the optimal values with the same number of quadrature points. Finally, for the 4D-basket put option under the NIG model, Figure 4.4a illustrates that, when using the optimal damping parameters, the TP quadrature crosses $\mathcal{E}_{\mathcal{R}} = 0.1\%$ using 22% of the work it would have used with damping parameters shifted by -2 in each direction w.r.t. the optimal values.

In summary, in all experiments, small shifts in both directions w.r.t. the optimal damping parameters lead to worse error convergence behavior, suggesting that the region of optimality of the damping parameters is tight and that our rule is sufficient to obtain optimal quadrature convergence behavior, independently of the quadrature method. Moreover, arbitrary choices of damping parameters may lead to extremely poor convergence of the quadrature, as illustrated by the purple curves in Figures 4.2a,4.2b, 4.3a and 4.4b. All compared damping parameters belong to the strip of regularity of the integrand δ_V defined in Section 2. Finally, although we only provide some plots to illustrate these findings, the same conclusions were consistently observed for different models and damping parameters.

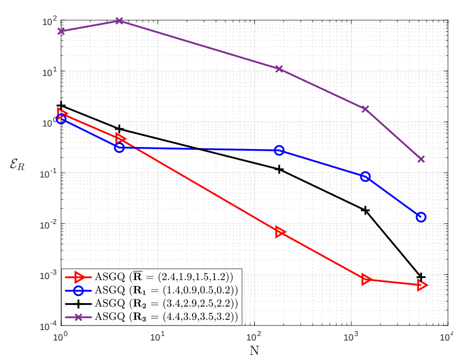

(a) Example 6 in Table 4.1

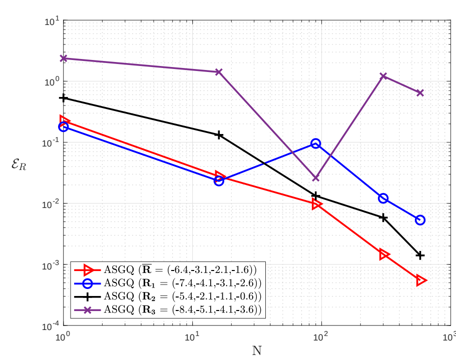

(b) Example 8 in Table 4.1

Figure 4.2: GBM model: Convergence of the relative quadrature error, $\mathcal{E}_R$, w.r.t. N for the ASGQ method for different damping parameter values.

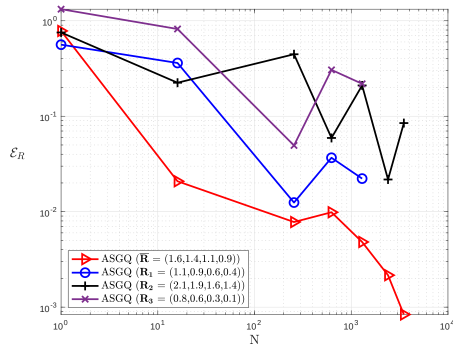

(a) Example 18 in Table 4.2

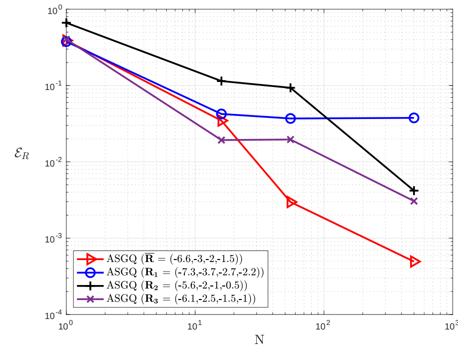

(b) Example 20 in Table 4.2

Figure 4.3: VG model: Convergence of the relative quadrature error, $\mathcal{E}_R$, w.r.t. N for the ASGQ method for different damping parameter values.

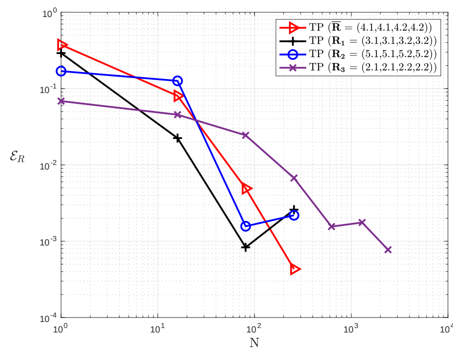

(a) Example 30 in Table 4.3

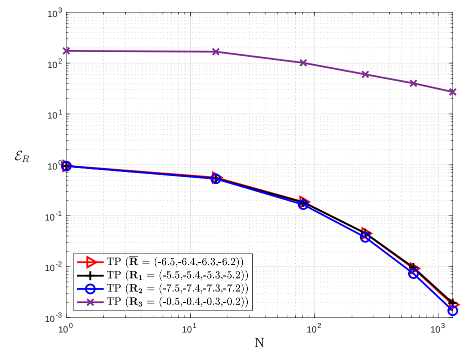

(b) Example 32 in Table 4.3

Figure 4.4: NIG model: Convergence of the relative quadrature error, $\mathcal{E}_R$, w.r.t. N for the TP method for different damping parameter values.

4.2 Computational comparison of quadrature methods with optimal damping and MC

This section compares the MC method and our proposed approach based on on the best quadrature method in the Fourier space combined with the optimal damping parameters in terms of errors and computational time. The comparison is performed for all option examples in Tables 4.1, 4.2, and 4.3. While fixing a sufficiently small relative error tolerance in the price estimates, we compare the necessary computational time for different methods to meet it in the following way:

1. Find the least number of quadrature points to reach a pre-defined relative quadrature error.
2. Estimate, using the CLT formula given in Equation (4.1), the required number of MC samples to achieve the same relative error achieved by the quadrature method.
3. Compare the CPU times of the both methods, including the cost of numerical optimization of (3.6) preceding the numerical quadrature for the Fourier approach. The MC CPU time is

obtained through an average of 10 runs.

The results presented in Table 4.4 highlight that our approach significantly outperforms the MC method for all the tested options with various models, parameter sets, and dimensions. In particular, for all tested 2D and 4D options, the proposed approach requires less than 20% (even less than 1% for most cases) of the MC work to achieve a total relative error below 0.1%. In general, these gains degrade for the tested 6D options. For Example 21 in Table 4.2, this approach requires around 43% of the work of MC, to achieve a total relative error below 1%. The magnitude of the CPU gain varies depending on different factors, such as the model and payoff parameters affecting the integrand differently in physical space (related to the MC estimator variance), and the integrand regularity in Fourier space (related to the quadrature error for quadrature methods). Finally, we observed significant memory gains using our approach for all examples, as we required considerably fewer quadrature points (functions evaluations) than the required number of samples for the MC method to meet the same error tolerance.

Acknowledgments C. Bayer gratefully acknowledges support from the German Research Foundation (DFG) via the Cluster of Excellence MATH+ (project AA4-2). This publication is based on the work supported by the King Abdullah University of Science and Technology (KAUST) Office of Sponsored Research (OSR) under Award No. OSR-2019-CRG8-4033 and the Alexander von Humboldt Foundation. Antonis Papapantoleon gratefully acknowledges the financial support from the Hellenic Foundation for Research and Innovation Grant No. HFRI-FM17-2152.

Declarations of Interest The authors report no conflicts of interest. The authors alone are responsible for the content and writing of the paper.

Example	**Best Quad**	$\mathcal{E}_{\mathcal{R}}$	**MC CPU Time**	M **(MC samples)**	**Quad CPU Time**	N **(Quad. Points)**	**CPU Time Ratio (Quad/MC) in %**
Example 1 in Table 4.1	ASGQ	$7e^{-04}$	7.36	1.2×10^7	0.63	33	8.5%
Example 2 in Table 4.1	ASGQ	$3.7e^{-04}$	20.7	3.3×10^7	0.65	67	3.14%
Example 13 in Table 4.2	TP	$2.9e^{-04}$	44	8.8×10^7	0.25	64	0.57%
Example 14 in Table 4.2	TP	$1.8e^{-04}$	70.9	1.4×10^8	0.23	64	0.32%
Example 25 in Table 4.3	TP	$2.9e^{-04}$	75.3	1.1×10^8	0.2	36	0.26%
Example 26 in Table 4.3	TP	$5.86e^{-04}$	17.2	2.6×10^7	0.2	25	1.16%
Example 3 in Table 4.1	ASGQ	$7e^{-04}$	47.3	7.6×10^7	0.6	37	1.26%
Example 4 in Table 4.1	ASGQ	$5.8e^{-04}$	102	1.4×10^8	0.63	37	0.62%
Example 15 in Table 4.2	ASGQ	$8.26e^{-04}$	19.5	4.1×10^7	0.54	25	2.77%
Example 16 in Table 4.2	TP	$5.37e^{-04}$	87.1	1.4×10^8	0.16	49	0.18%
Example 26 in Table 4.3	TP	$6.7e^{-04}$	35.8	5.3×10^7	0.22	100	0.61%
Example 27 in Table 4.3	TP	$6.46e^{-04}$	42.2	6.5×10^7	0.22	64	0.52%
Example 5 in Table 4.1	ASGQ	$2.46e^{-04}$	207	10^8	7.8	5257	3.77%
Example 6 in Table 4.1	ASGQ	$8.12e^{-04}$	14.5	7.9×10^6	2.73	1433	18.83%
Example 17 in Table 4.2	ASGQ	$2.58e^{-04}$	106.3	1.23×10^8	5	3013	4.7%
Example 18 in Table 4.2	ASGQ	$3.58e^{-04}$	38.7	4.5×10^7	2	1109	5.17%
Example 27 in Table 4.3	TP	$4.57e^{-04}$	50.2	4.7×10^7	0.5	256	1%
Example 28 in Table 4.3	TP	$4.1e^{-04}$	49.4	4.8×10^7	0.52	256	1%
Example 7 in Table 4.1	ASGQ	$5.7e^{-04}$	1147	7×10^8	1	435	0.09%
Example 8 in Table 4.1	ASGQ	$5.5e^{-04}$	1580	9.6×10^8	0.95	654	0.06%
Example 19 in Table 4.2	ASGQ	$5.9e^{-04}$	220	3×10^8	1.25	567	0.57%
Example 20 in Table 4.2	ASGQ	$8.9e^{-04}$	249	3.3×10^8	1.4	862	0.56%
Example 29 in Table 4.3	TP	$7.2e^{-04}$	193.5	2×10^8	8.7	20736	4.5%
Example 30 in Table 4.3	TP	$4.2e^{-04}$	716	7.8×10^8	0.8	2401	0.11%
Example 9 in Table 4.1	ASGQ	$2.9e^{-02}$	18.53	5.5×10^6	2	318	11%
Example 10 in Table 4.1	ASGQ	$3.3e^{-03}$	548	1.5×10^8	2.1	340	0.38%
Example 21 in Table 4.2	ASGQ	$7.8e^{-03}$	5.4	4.7×10^6	2.3	453	42.6%
Example 22 in Table 4.2	ASGQ	$5.4e^{-03}$	31.5	2.5×10^7	3.5	566	11%
Example 31 in Table 4.3	ASGQ	$1.47e^{-02}$	14.2	10^7	3.4	616	24%
Example 32 in Table 4.3	TP	$3.75e^{-02}$	33.5	2.5×10^7	11.7	4096	35%
Example 11 in Table 4.1	ASGQ	$1.4e^{-03}$	2635	6.9×10^8	6	3070	0.23%
Example 12 in Table 4.1	ASGQ	$1.7e^{-03}$	2110	5.3×10^8	4.5	1642	0.21%
Example 23 in Table 4.2	ASGQ	$2e^{-03}$	85	6.8×10^7	19.5	7401	23%
Example 24 in Table 4.2	ASGQ	$2.6e^{-03}$	360	2.8×10^8	4.6	1671	1.28%
Example 33 in Table 4.3	ASGQ	$5.7e^{-02}$	85.5	6.3×10^7	1	105	1.17%
Example 34 in Table 4.3	ASGQ	$3.79e^{-02}$	108	7.5×10^7	1.4	340	1.3%

Table 4.4: Errors, CPU times, and function evaluations comparing the Fourier approach combined with the optimal damping rule and the best quadrature (Quad) method with the Gauss–Laguerre rule against the MC method for the European basket and rainbow options under the multivariate GBM, VG, and NIG pricing dynamics for various dimensions. Tables 4.1, 4.2, 4.3 present the selected parameter sets for each pricing model, the reference values with their corresponding statistical errors, and the optimal damping parameters.

References Cited

[1] Jean-Philippe Aguilar. Some pricing tools for the variance Gamma model. *International Journal of Theoretical and Applied Finance*, 23(04):2050025, 2020.

[2] Ivo Babuška, Fabio Nobile, and Raúl Tempone. A stochastic collocation method for elliptic partial differential equations with random input data. *SIAM Journal on Numerical Analysis*, 45(3):1005–1034, 2007.

[3] Ole E Barndorff-Nielsen. Processes of normal inverse Gaussian type. *Finance and Stochastics*, 2(1):41–68, 1997.

[4] Volker Barthelmann, Erich Novak, and Klaus Ritter. High dimensional polynomial interpolation on sparse grids. *Advances in Computational Mathematics*, 12(4):273–288, 2000.

[5] Fabio Baschetti, Giacomo Bormetti, Silvia Romagnoli, and Pietro Rossi. The sinc way: a fast and accurate approach to Fourier pricing. *Quantitative Finance*, pages 1–20, 2021.

[6] Christian Bayer, Chiheb Ben Hammouda, and Raúl Tempone. Hierarchical adaptive sparse grids and Quasi-Monte Carlo for option pricing under the rough Bergomi model. *Quantitative Finance*, 20(9):1457–1473, 2020.

[7] Christian Bayer, Chiheb Ben Hammouda, and Raul Tempone. Numerical smoothing and hierarchical approximations for efficient option pricing and density estimation. *arXiv preprint arXiv:2003.05708*, 2020.

[8] Christian Bayer, Chiheb Ben Hammouda, and Raúl Tempone. Numerical smoothing with hierarchical adaptive sparse grids and quasi-Monte Carlo methods for efficient option pricing. *arXiv preprint arXiv:2111.01874*, 2021.

[9] Christian Bayer, Markus Siebenmorgen, and Raúl Tempone. Smoothing the payoff for efficient computation of basket option prices. *Quantitative Finance*, 18(3):491–505, 2018.

[10] Chiheb Ben Hammouda. *Hierarchical Approximation Methods for Option Pricing and Stochastic Reaction Networks*. PhD thesis, 2020.

[11] Richard H Byrd, Jean Charles Gilbert, and Jorge Nocedal. A trust region method based on interior point techniques for nonlinear programming. *Mathematical programming*, 89(1):149–185, 2000.

[12] Richard H Byrd, Mary E Hribar, and Jorge Nocedal. An interior point algorithm for large-scale nonlinear programming. *SIAM Journal on Optimization*, 9(4):877–900, 1999.

[13] Peter Carr and Dilip Madan. Option valuation using the fast Fourier transform. *Journal of Computational Finance*, 2(4):61–73, 1999.

[14] Peter Carr and Liuren Wu. Time-changed Lévy processes and option pricing. *Journal of Financial Economics*, 71:113–141, 2004.

[15] Peng Chen. Sparse quadrature for high-dimensional integration with gaussian measure. *ESAIM: Mathematical Modelling and Numerical Analysis*, 52(2):631–657, 2018.

[16] Jaehyuk Choi. Sum of all Black–Scholes–Merton models: An efficient pricing method for spread, basket, and Asian options. *Journal of Futures Markets*, 38(6):627–644, 2018.

[17] Rama Cont and Peter Tankov. *Financial Modelling with Jump Processes*. Chapman and Hall/CRC, 2003.

[18] Ricardo Crisóstomo. Speed and biases of Fourier-based pricing choices: a numerical analysis. *International Journal of Computer Mathematics*, 95(8):1565–1582, 2018.

[19] Philip Davis and Philip Rabinowitz. On the estimation of quadrature errors for analytic functions. *Mathematical Tables and Other Aids to Computation*, 8(48):193–203, 1954.

[20] Philip J. Davis and Philip Rabinowitz. *Methods of Numerical Integration*. Courier Corporation, 2007.

[21] J.D. Donaldson. Estimates of upper bounds for quadrature errors. *SIAM Journal on Numerical Analysis*, 10(1):13–22, 1973.

[22] J.D. Donaldson and David Elliott. A unified approach to quadrature rules with asymptotic estimates of their remainders. *SIAM Journal on Numerical Analysis*, 9(4):573–602, 1972.

[23] Darrell Duffie, Damir Filipović, and Walter Schachermayer. Affine processes and applications in finance. *The Annals of Applied Probability*, 13(3):984–1053, 2003.

[24] Ernst Eberlein, Kathrin Glau, and Antonis Papapantoleon. Analysis of Fourier transform valuation formulas and applications. *Applied Mathematical Finance*, 17(3):211–240, 2010.

[25] David Elliott. Uniform asymptotic expansions of the classical orthogonal polynomials and some associated functions. In *Technical Report No. 21*. Mathematics Department, The University of Tasmania Hobart, Tasmania, 1970.

[26] David Elliott and P.D. Tuan. Asymptotic estimates of Fourier coefficients. *SIAM Journal on Mathematical Analysis*, 5(1):1–10, 1974.

[27] Fang Fang and Cornelis. W. Oosterlee. A novel pricing method for European options based on Fourier-cosine series expansions. *SIAM Journal on Scientific Computing*, 31(2):826–848, 2008.

[28] Walter Gautschi. *Orthogonal Polynomials: Computation and Approximation*. OUP Oxford, 2004.

[29] Thomas Gerstner and Michael Griebel. Numerical integration using sparse grids. *Numerical Algorithms*, 18(3):209–232, 1998.

[30] Thomas Gerstner and Michael Griebel. Dimension–adaptive tensor–product quadrature. *Computing*, 71:65–87, 2003.

[31] Paul Glasserman. *Monte Carlo Methods in Financial Engineering*, volume 53. Springer, 2004.

[32] Tristan Guillaume. Making the best of best-of. *Review of Derivatives Research*, 11(1):1–39, 2008.

[33] Jherek Healy. The pricing of vanilla options with cash dividends as a classic vanilla basket option problem. *arXiv preprint arXiv:2106.12971*, 2021.

[34] Thomas R Hurd and Zhuowei Zhou. A Fourier transform method for spread option pricing. *SIAM Journal on Financial Mathematics*, 1(1):142–157, 2010.

[35] Gero Junike and Konstantin Pankrashkin. Precise option pricing by the cos method—how to choose the truncation range. *Applied Mathematics and Computation*, 421:126935, 2022.

[36] Christian Kahl and Roger Lord. Fourier inversion methods in finance. *Handbook of Computational Finance*, 2010.

[37] J. Lars. Kirkby. Efficient option pricing by frame duality with the fast Fourier transform. *SIAM Journal on Financial Mathematics*, 6(1):713–747, 2015.

[38] Yue Kuen Kwok, Kwai Sun Leung, and Hoi Ying Wong. Efficient options pricing using the fast Fourier transform. In *Handbook of Computational Finance*, pages 579–604. Springer, 2012.

[39] Roger. W. Lee. Option pricing by transform methods: extensions, unification, and error control. *Journal of Computational Finance*, 7(3):50–86, 2004.

[40] C.C.W. Leentvaar and Cornelis. W. Oosterlee. Multi-asset option pricing using a parallel Fourier-based technique. *Journal of Computational Finance*, 12(1):1, 2008.

[41] Alan L. Lewis. A simple option formula for general jump-diffusion and other exponential lévy processes. *Available at SSRN 282110*, 2001.

[42] Roger Lord, Fang Fang, Frank Bervoets, and Cornelis. W. Oosterlee. A fast and accurate FFT-based method for pricing early-exercise options under lévy processes. *SIAM Journal on Scientific Computing*, 30(4):1678–1705, 2008.

[43] Roger Lord and Christian Kahl. Optimal Fourier inversion in semi-analytical option pricing. 2007.

[44] Elisa Luciano and Wim Schoutens. A multivariate jump-driven financial asset model. *Quantitative finance*, 6(5):385–402, 2006.

[45] Dilip B. Madan and Eugene Seneta. The variance Gamma (V.G.) model for share market returns. *The Journal of Business*, 63:511–524, 1990.

[46] William Margrabe. The value of an option to exchange one asset for another. *The journal of finance*, 33(1):177–186, 1978.

[47] Johannes Muhle-Karbe, Oliver Pfaffel, and Robert Stelzer. Option pricing in multivariate stochastic volatility models of ou type. *SIAM Journal on Financial Mathematics*, 3(1):66–94, 2012.

[48] C. Piazzola and L. Tamellini. The Sparse Grids Matlab kit - a Matlab implementation of sparse grids for high-dimensional function approximation and uncertainty quantification. *ArXiv*, (2203.09314), 2022.

[49] Sebastian Raible. *Lévy processes in finance: Theory, numerics, and empirical facts.* PhD thesis, Universität Freiburg i. Br, 2000.

[50] Marjon J Ruijter and Cornelis. W. Oosterlee. Two-dimensional Fourier cosine series expansion method for pricing financial options. *SIAM Journal on Scientific Computing*, 34(5):B642–B671, 2012.

[51] Martin Schmelzle. Option pricing formulae using Fourier transform: Theory and application. *Preprint, http://pfadintegral. com*, 2010.

[52] Wim Schoutens. *Lévy Processes in Finance: Pricing Financial Derivatives.* Wiley Online Library, 2003.

[53] Sergei Abramovich Smolyak. Quadrature and interpolation formulas for tensor products of certain classes of functions. In *Doklady Akademii Nauk*, volume 148, pages 1042–1045. Russian Academy of Sciences, 1963.

[54] Hidetosi Takahasi and Masatake Mori. Estimation of errors in the numerical quadrature of analytic functions. *Applicable Analysis*, 1(3):201–229, 1971.

[55] Edward Charles Titchmarsh et al. *Introduction to the Theory of Fourier Integrals*, volume 2. Clarendon Press Oxford, 1948.

[56] Lloyd N Trefethen. Is Gauss quadrature better than Clenshaw–Curtis? *SIAM Review*, 50(1):67–87, 2008.

[57] Dennis van de Wiel. Valuation of insurance products using a normal inverse Gaussian distribution. Bachelor's thesis, 2015.

[58] Grzegorz W. Wasilkowski and Henryk Wozniakowski. Explicit cost bounds of algorithms for multivariate tensor product problems. *Journal of Complexity*, 11(1):1–56, 1995.

[59] Shuhuang Xiang. Asymptotics on Laguerre or Hermite polynomial expansions and their applications in Gauss quadrature. *Journal of Mathematical Analysis and Applications*, 393(2):434–444, 2012.

[60] Bowen Zhang and Cornelis W. Oosterlee. Efficient pricing of European-style Asian options under exponential Lévy processes based on Fourier cosine expansions. *SIAM Journal on Financial Mathematics*, 4(1):399–426, 2013.

[61] Jianwei Zhu. *Applications of Fourier Transform to Smile Modeling: Theory and Implementation.* Springer Science & Business Media, 2009.

A Option Pricing Models in Physical Space

In this section, we briefly give the details of the pricing models considered in this work: the multivariate GBM (Section A.1), VG (Section A.2.1), and NIG (Section A.2.2) models.

A.1 Multivariate Geometric Brownian Motion

In the multivariate GBM model with d assets $\{S_i(.)\}_{i=1}^d$, each stock satisfies[7]

$$S_i(t) \stackrel{d}{=} S_i(0) \exp\left[\left(r - \frac{\sigma_i^2}{2}\right) t + \sigma_i W_i(t)\right], \quad i = 1, \ldots, d, \tag{A.1}$$

where $\sigma_1, \ldots, \sigma_d > 0$ and $\{W_1(t), \ldots, W_d(t), t \geq 0\}$ are independent standard Brownian motions with correlation matrix $\mathbf{C} \in \mathbb{R}^{d\times d}$ with components $-1 \leq \rho_{i,j} \leq 1$, denoting the correlation between W_i and W_j. Moreover, $\mathbf{\Sigma} \in \mathbb{R}^{d\times d}$ denotes the covariance matrix of the log returns, $\{\log(\frac{S_i(t)}{S_i(0)})\}_{i=1}^d$, with $\mathbf{\Sigma}_{ij} = \rho_{i,j}\sigma_i\sigma_j$.

A.2 Multivariate Lévy models

Many stock price models are of the form $S_i(t) \stackrel{d}{=} S_i(0)e^{(r+\mu_i)t+X_i(t)}$, where $X_i(t)$ is a Lévy process, for which the characteristic function is explicitly known, μ_i is the Martingale correction term. We consider two models within this family: the VG and NIG models in Sections A.2.1 and A.2.2, respectively.

A.2.1 Multivariate variance Gamma

We consider the multivariate VG model introduced in [44]. The joint risk-neutral dynamics of the stock prices are modeled as follows:

$$S_i(t) \stackrel{d}{=} S_i(0) \exp\left\{(r + \mu_{VG,i})\, t + \theta_i G(t) + \sigma_i \sqrt{G(t)} W_i(t)\right\}, \quad i = 1, \ldots, d, \tag{A.2}$$

where $\{W_1(t), \ldots, W_d(t)\}$ are independent standard Brownian motions, $\{G(t)|t \geq 0\}$ is a common Gamma process with parameters (a, b) defined by the pdf, $f_G(x; a, b) = \frac{b^{at}}{\Gamma(at)} x^{at-1}e^{-bx}$, $x \geq 0$, independent of all involved Brownian motions, with parameters $(\frac{t}{\nu}, \frac{1}{\nu})$. $\theta_i \in \mathbb{R}$ and $\sigma_i > 0$, $1 \leq i \leq d$. We only consider the case in which the Brownian motions of the stocks are uncorrelated and share the same parameter ν; thus, the matrix $\mathbf{\Sigma} \in \mathbb{R}^{d\times d}$, presented in Table 2.1 satisfies $\Sigma_{i,j} = {\sigma_i}^2$ for $i = j$, and 0 otherwise. In addition, $\boldsymbol{\mu}_{VG} := (\mu_{VG,1}, \ldots, \mu_{VG,d})$ are the Martingale correction terms that ensure that $\{e^{-rt}S_i(t)|t \geq 0\}$ is a Martingale and are given by

$$\mu_{VG,i} = \frac{1}{\nu} \log\left(1 - \frac{1}{2}\sigma_i^2\nu - \theta_i\nu\right), \quad i = 1, \ldots, d. \tag{A.3}$$

A.2.2 Multivariate normal inverse Gaussian

We consider the multivariate NIG model where the joint risk-neutral dynamics of the stock prices are modeled as follows:

$$S_i(t) \stackrel{d}{=} S_i(0) \exp\left\{(r + \mu_{NIG,i})\, t + \beta_i IG(t) + \sqrt{IG(t)} W_i(t)\right\}, \quad i = 1, \ldots, d, \tag{A.4}$$

where $\{W_1(t), \ldots, W_d(t)\}$ are independent standard Brownian motions, $\{IG(t)|t \geq 0\}$ is a common inverse Gaussian process with parameters (a, b) defined by the pdf, $f_{IG}(x; a, b) = \left(\frac{a}{2\pi x^3}\right)^{1/2} e^{\frac{-a(x-b)^2}{2b^2x}}$, $x >$

[7] $\stackrel{d}{=}$ denotes the equality in distribution.

0, independent of all involved Brownian motions with parameters $(\delta^2 t^2, \alpha^2 - \boldsymbol{\beta}^{\mathrm{T}}\boldsymbol{\Delta}\boldsymbol{\beta})$. Additionally, $\alpha \in \mathbb{R}_+$, $\boldsymbol{\beta} \in \mathbb{R}^d$, $\alpha^2 > \boldsymbol{\beta}^{\mathrm{T}}\boldsymbol{\Delta}\boldsymbol{\beta}$, $\delta > 0$, and $\boldsymbol{\Delta} \in \mathbb{R}^{d\times d}$ is a symmetric positive definite matrix with a unit determinant. $\{\mu_{NIG,i}\}_{i=1}^{d}$ are the Martingale correction terms that ensure that $\{e^{-rt}S_i(t)|t \geq 0\}$ is a Martingale, given by

$$\mu_{NIG,i} = -\delta\left(\sqrt{\alpha^2-\beta_i^2} - \sqrt{\alpha^2-(\beta_i+1)^2}\right), \quad i = 1,\ldots,d. \tag{A.5}$$

B On the Choice of the Quadrature Rule

In this section, through numerical examples on vanilla put options, we show that the Gauss–Laguerre quadrature rule significantly outperforms the Gauss–Hermite quadrature rule for the numerical evaluation of the inverse Fourier integrals; hence, we adopt the Gauss–Laguerre measure for the rest of the work. Figures B.1a, B.1b, and B.1c reveal that the Gauss–Laguerre quadrature rule significantly outcompetes the Gauss–Hermite quadrature independently of the values of the damping parameters in the strip of regularity for the tested models: GBM, VG, and NIG. For instance, Figure B.1a illustrates that, when $R = 4$ is used, the Gauss–Laguerre quadrature rule reaches approximately the relative quadrature $\mathcal{E}_R = 0.01\%$ using 12% of the work required by the Gauss–Hermite quadrature to attain the same accuracy. These observations were consistent for all tested parameter constellations and dimensions, and independent of the choice of the quadrature methods (TP, ASGQ, or SM).

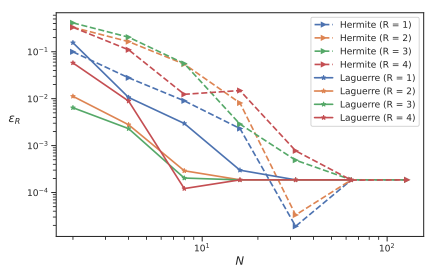

(a) $\sigma = 0.4$

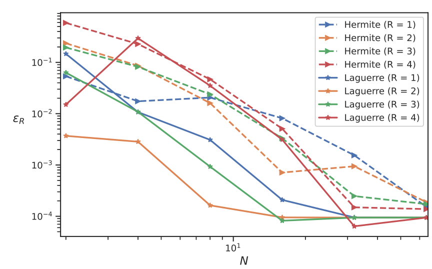

(b) $\sigma = 0.4, \theta = -0.3, \nu = 0.257$

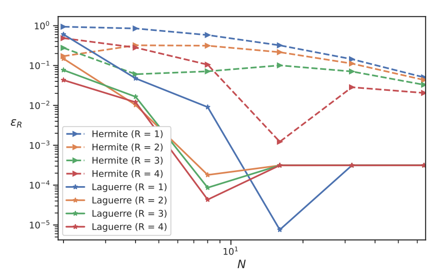

(c) $\alpha = 10, \beta = -3, \delta = 0.2$

Figure B.1: Relative quadrature error, $\mathcal{E}_R$, convergence w.r.t. N of Gauss–Laguerre and Gauss–Hermite quadrature rules for a European put option with $S_0 = 100$, $K = 100$, $r = 0$, and $T = 1$ under (a) GBM, (b) VG, and (c) NIG.